er, private communication.
[20]J. W. Meadows, Phys. Rev. 91, 885 (1953).
[21]J. Hudis, CERN NP DIV. Internal Report No. 68-22, 1968 (unpublished); private communication.
[22]G. Rudstam, Z. Naturforsch, 21a, 1027 (1966).
[23]K. Chen, Z. Fraenkel, G. Friedlander, J. R. Grover, J. M. Miller, and Y. Shimamoto, Phys. Rev. 166, 949 (1968).
[24]I. Dostrovsky, Z. Fraenkel, and G. Friedlander, Phys. Rev. 116, 683 (1960).
[25]Such an observation is not inconsistent with the results reported by Rudstam (1966) for Cu as target at similar projectile energies. However, Brodzinski *et al.* [Phys. Rev. C 4, 1250, 1257 (1971)] recently reported that the Rudstam approach provided systematically higher cross-section estimates than their own experimental values for various products in Ti and Fe targets irradiated with protons of comparable energy to those employed in this work.
[26]Although experimental values should be systematically higher than those predicted by the calculations due to contributions to the former from short-lived precursors, such effects are of insufficient magnitude to be important here.
[27]Since the range of products studied in this work is confined to those rather close to stability, the relative performances of the two calculational techniques for other products (or projectile energies or targets) can not, necessarily, be inferred from those encountered here.

PHYSICAL REVIEW C VOLUME 6, NUMBER 4 OCTOBER 1972

Variation of the ^{32}S Compound-Nucleus Width with Energy and Spin*

R. B. Leachman,† P. Fessenden,‡ and W. R. Gibbs
Los Alamos Scientific Laboratory, University of California, Los Alamos, New Mexico 87544
(Received 29 November 1971)

Coherence widths of the compound nucleus ^{32}S were determined from excitation functions of the differential cross section for the reactions ^{31}P(p,α)^{28}Si and ^{16}O(^{16}O,α)^{28}Si. The proton-induced reaction provided a lower average spin of the compound nucleus. Excitation functions were measured for ^{31}P(p,α)^{28}Si from 13.90- to 14.24- and from 26.62- to 30.56-MeV compound-nucleus energy. The average coherence widths were 11 ± 1.2 and 95 ± 15 keV, respectively. For the oxygen-induced reaction, excitation functions were measured from 28.99 to 34.42 MeV with a resulting 73 ± 7-keV coherence width, which is nearly the same as for the lower-spin proton-induced case.

These coherence widths were used to test the Gilbert and Cameron level-density formulation. Good agreement with the above data was obtained if the compound nucleus ^{32}S is considered to be spherical in this formulation. The increase in the calculated width for the ^{16}O induced reaction with increasing excitation energy is greater than indicated by combining our data with another measurement at higher excitation.

I. INTRODUCTION

Information on the level densities $\rho(E, J)$ of nuclei as a function of excitation energy E and spin J has several uses. Gadioli and Zetta[1] note that measurements of level widths are the main method of determining densities for $E \gtrsim 6$ MeV, while for lower energies more direct and quantitative methods are available. The present work is an extensive investigation of the compound nucleus ^{32}S at excitation energies from 14 up to 34 MeV. The span of spin conditions in the reactions studied and the span of energies covered combine to make this a particularly rich collection of data on which to test energy and spin dependence of level-density expressions.

Experimentally, the present studies were measurements of excitation functions made in sufficiently small steps of incident energy and with sufficiently good resolution to permit fluctuation analyses.[2] Use of the compound nucleus ^{32}S provided several advantages:

(1) The minimum spin $\frac{1}{2}$ of both the proton and the target nucleus ^{31}P allow use of the convenient reaction ^{31}P(p, α)^{28}Si as the low-spin case for the study of the intermediate nucleus ^{32}S.

(2) The nucleus ^{32}S has a sufficiently large mass number that levels have the necessary overlap[3] at 14-MeV excitation energy, but has a sufficiently small mass number that the cross section for ^{16}O(^{16}O, α)^{28}Si at 34-MeV excitation energy is adequate to allow fluctuation measurements. This allows a large span of energies.

(3) Other fluctuation measurements have been reported for the compound nucleus ^{32}S. Measurements have been made of the ^{31}P(p, α)^{28}Si reaction at intermediate energies,[4,5] the ^{16}O(^{16}O, α)^{28}Si reaction and ^{16}O-^{16}O scattering at a slightly higher

energy,[6] the ^{28}Si(α, α')^{28}Si* reaction at intermediate energies,[7] and the ^{31}P(p, p)^{31}P reaction at an intermediate energy.[8]

Other compound nuclei have also been studied by fluctuation measurements with various reactions, but with smaller energy spans and with more complex conditions of spin. As one example, the compound nucleus ^{24}Mg has been studied by the ^{12}C-(^{12}C, α)^{20}Ne reaction,[9,10] and by the ^{23}Na(p, α)^{20}Ne reaction.[11] The former resulted in a 120-keV coherence width Γ at 25.4-MeV compound-nucleus excitation energy[10]; all spins are zero. The latter resulted in 110-keV coherence width at 20.8-MeV excitation energy[11]; the target spin is $\frac{3}{2}$. Although energies are somewhat different and target spins are not the same, the widths are similar. As a more complete example, the compound nucleus ^{28}Si has been studied extensively by fluctuation analyses.[12-14] The energy span covered has been somewhat less than for the present case of ^{32}S and the $\frac{5}{2}$ spin of the target nucleus of the ^{27}Al(p, α)-^{24}Mg reaction complicates the effort to have low compound-nucleus spin by proton bombardment.

We now consider the use of widths Γ from fluctuation analyses to test models of the statistical level densities ρ of nuclei for excitation energies above about 6 MeV. These tests have previously[6,7] been used for the ^{32}S compound nucleus, but are considered in greater detail in the present paper. The tests have been used extensively for the ^{28}Si compound nucleus.[7,13,14] The method of fluctuation averaging[15] has allowed tests of the statistical model for nuclei as heavy as ^{116}Sn.

These tests of the statistical model of level densities by fluctuation widths follow the mnemonic $2\pi\langle\Gamma\rangle/\langle D\rangle = \sum T_l$. In correct detail, widths are calculated by

$$2\pi\Gamma_J^{\nu}/D_{\mathrm{CN}}^{\nu} = \sum_I \sum_{j=|J-I|}^{J=I} \sum_{l=j-s}^{j+s} \times \int_0^{E_{\mathrm{CN}}-Q} dE\, \rho_r(E_{\mathrm{CN}} - Q - E, I) T_{l,j}(E), \quad (1)$$

where ν is the exit-particle identity (protons, neutrons, α particles, or ^{16}O), Q is the binding energy of that particle to the compound nucleus, ρ_r is the level density of the residual nucleus, $\rho_{\mathrm{CN}} = (D_{\mathrm{CN}})^{-1}$ is the level density of the compound nucleus, and $T_{l,j}(E)$ is the transmission coefficient for the emitted particle of energy E and orbital (total) angular momentum $l(j)$. The spin of the emitted particle is s, and the nuclear spin of the residual nucleus is designated by I. For each value of total spin J, the width is obtained by summation over the widths associated with each particle identity, $\Gamma_J = \sum_\nu \Gamma_J^{\nu}$. The width Γ which is to be compared with the observed width from fluctuation measurements is obtained from[16]

$$\Gamma = \sum_J \sigma_J / \sum_J (\sigma_J/\Gamma_J), \quad (2)$$

where the σ_J are partial cross sections calculated by the Hauser-Feshbach approximation.[17]

Determining the level densities $\rho(E, I)$ for both the residual nuclei and the compound nucleus is the central problem in comparing the width calculated by (1) and (2) with the width measured by fluctuations. Unfortunately, the free choices in the level-density parametrization often exceed the number of datum points of width. These choices are often between: the constant temperature or Fermi gas expression; the nuclear temperature or the level-density parameter a; the pairing energies; any "backward shifting"[1,4]; effect of nuclear deformation on level density; and the moment of inertia $\mathcal{I}$ in the dependence of the level density on nuclear spin I or J.[18]

Several different approaches have been used to cope with these uncertainties in the level-density expressions. In their comparison with fluctuation widths from medium-weight elements, Fessenden, Gibbs, and Leachman[15] use the explicit level-density parametrization given by Gilbert and Cameron,[19] which is a combination of constant temperature for lower excitations and Fermi gas for higher and utilizes fits to data for each nuclide. More commonly, a Fermi-gas expression has been used and variations on the several free parameters have been tried.[1,4,6,7,13] Eberhard and Richter[14] utilized a closed form for the width which was obtained from simplifications in the level-density expression and a sharp cutoff model of transmission coefficients.[20] Again, fits were made for parameters.

Comparisons between these various calculated results could be misleading for two reasons. First, inspection of (1) shows that the calculated width Γ is qualitatively a function of the ratio between the level density ρ_r of residual nuclei and the level density ρ_{CN} of the compound nucleus. Since residual nuclei and the compound nuclei have nearly equal mass, the level-density parametrizations are expected to be similar. Consequently, subtle changes in parametrizations of ρ_r and ρ_{CN}, not gross changes, play the dominant role in calculating widths with (1). Second, in the actual calculations of width with (1), the great detail in transmission coefficients $T_{l,j}$ and in the sums makes comparisons between calculations with different parametrizations difficult.

As a consequence of the different parametrizations used[1,4,6,7,13,14] and this difficulty in intercom-

parisons, establishing a trend from these results would be dangerous. Instead, in the present study, calculations are made with the level-density expression of Gilbert and Cameron,[19] which has essentially all parameters fixed by comparison with lower-energy data. These calculated results are tested in Sec. V against the ^{32}S widths from fluctuation measurements, which have unusually great span in excitation energy and in compound-nucleus spin.

II. EXPERIMENTAL PROCEDURE

The considerably different energies and incident particles used in the present study necessitated varied experimental arrangements.

A. Low-Energy $^{31}P(p, \alpha)^{28}Si$ Reactions

For the measurements with low-energy protons, a previously described[21, 22] arrangement was used for measuring the differential cross section to three laboratory angles of 130, 150, and 170°. In the present case, counters subtended 4 to 6° angular spans.

The ^{31}P target[23] was 13.8 ± 1.1 $\mu g/cm^2$ deposited by an isotope separator on a 0.1-mg/cm^2 carbon foil. Protons were from a single-stage Van de Graaff at about 0.1-μA current and in 2.5-keV increments increasing in energy from 5.20 to 5.55 MeV. To minimize the pulse size from scattered protons, thin semiconductor detectors of 45- to 77-μ thickness were used. α particles leading to the 0^+ ground state and 2^+ first excited state of ^{28}Si were detected. (Experimental difficulties required rejection of most of the 150° first excited state data.)

B. High-Energy $^{31}P(p, \alpha)^{28}Si$ Reactions

To provide compound-nucleus excitation energies comparable to those from the lowest-energy oxygen-induced reaction, about 20-MeV protons are needed. These were from a three-stage Van de Graaff. Energy increments of 20 keV were used between 18.4 and 22.4 MeV. (About one third of this interval was covered in 10-keV increments, but without any increase in cross-section structure.) Currents were about 0.35 μA.

For these higher energies a target of 37 ± 2 $\mu g/cm^2$ phosphorus was used. The phosphorus was deposited from the vapor phase on a cooled carbon foil of 30 $\mu g/cm^2$.[23]

The large number of competing exit channels in the reaction at these higher energies resulted in $^{31}P(p, \alpha)^{28}Si$ cross sections that are two or three orders of magnitude lower than for the low-energy reaction. Therefore, a particular effort was required to increase the solid angle of detection to provide a reasonably short observation time for the individual fluctuation-data runs. A 50-cm scattering chamber was used with the target mounted perpendicular to the beam, which was collimated to a 0.4-cm diameter. Six detectors were used at the 133° (lab) angle of measurement. These were surface-barrier detectors, with aluminum absorber foils, mounted along a collimator system that was a 7.9°-wide spherical zone at 133°. The spherical zone was concentric with the beam axis, and the six detectors collectively subtended 0.17 sr from the target. A monitor detector placed at 15° indicated no target deterioration.

Angular distributions were measured by a conventional detector set up in a horizontal plane. These detectors subtended 6.5° angles from the target.

C. $^{16}O(^{16}O, \alpha)^{28}Si$ Reactions

Even greater detection rate difficulties were encountered for the oxygen-induced reaction. Here, the cross section is similarly small, but the problems of target thickness, angular acceptance, and beam currents are greater. The considerably greater rate of energy loss for oxygen ions compared to protons necessitates very thin targets to result in an energy loss that is not larger than the coherence width being measured. The complex structure of angular distributions from heavy-ion induced reactions[9, 10, 13, 24] requires the angle subtended from the target to be small. Accelerator ion-source capabilities limit the ^{16}O-ion current available.

For good resolution measurements, a target of a 7.0 ± 1.4 $\mu g/cm^2$ WO_3 deposited on a 30-$\mu g/cm^2$ carbon backing was used. The thickness was determined by relative cross-section measurements with a thicker target which was weighed. The thickness of the 7-$\mu g/cm^2$ target was 27 keV (lab) for 27-MeV (lab) oxygen ions. In detailed measurements this target displayed no more cross-section structure in excitation-function measurements than did 17-$\mu g/cm^2$ WO_3 and 30-$\mu g/cm^2$ Ta_2O_5 targets. (This is consistent with the 73-keV coherence width determined below.) The 7.0-$\mu g/cm^2$ WO_3 target was used with 24.9- to 29.2-MeV oxygen energies (lab) in 50-keV energy (lab) increments. In addition, a self-supporting 40-$\mu g/cm^2$ SiO target, for which the 208-keV (lab) oxygen-ion energy loss is roughly equal to the coherence width, was used for measuring the excitation function in 150-keV (lab) energy increments from 25.0 to 35.75 MeV (lab) for 73° (lab) and from 29.20 to 35.75 MeV (lab) for 176° (lab).

The two-stage tandem Van de Graaff was used to

provide beams of $^{16}O^{++++}$ at generally 0.2 μA. The current was measured by a Faraday cup after having passed through the target. Beam-current measurements with the target in and the target out established that the target stripped the oxygen ions to 6.2 ± 0.3 ionic charge.

Frequent repeats of cross-section measurement at a calibration energy were used to detect any change of the oxygen content of the target. A slow decrease of oxygen in the 7-μg/cm^2 WO_3 target with bombardment time was found. The SiO target did not change. The target spot on the WO_3 target was shifted frequently, and small corrections were made to compensate for oxygen decrease during bombardments. Reactions with other elements in the target produced α particles of similar energies, particularly for $^{13}C(^{16}O, \alpha)^{25}Mg$. However, these were readily resolved from the α particles of interest.

To minimize the number of independent amplitudes, excitation functions at 90°(c.m.) and close to 0 or 180° are desirable. In principle, measurements at 0° are possible by the method[9, 10, 24] of using a beam absorber in front of the 0° counter. For $^{16}O(^{16}O, \alpha)^{28}Si$ measurements, difficulties of oxygen buildup on the absorber were troublesome, and so measurements were instead made at the extreme backward angle. An annular surface-barrier detector with a 1-cm i.d. and a 2-cm o.d. was used at 176° (lab), or 177° (c.m.) subtending a 3° angle and 0.016 sr from the target. A 0.01-cm-thick aluminum foil was used in front of the 120-μ depletion-depth detector to degrade the α particles sufficiently to stop in the detector.

In an arrangement similar to that in Sec. II B, six detectors were used along a 73° (lab), or 90° (c.m.), spherical zone that was 4° wide. For the excitation functions with the 7-μg/cm^2 WO_3 target at lower energies, 300-μ surface-barrier detectors covered by 0.003 cm Al were used with a total solid angle of 0.08 sr. For measurements with the 40-μg/cm^2 SiO target at higher energies, small area 2-mm-thick lithium-drifted silicon counters were used subtending a total solid angle of 0.02 sr.

For angular distributions, the maximum angle subtended by detectors was 2.6°. The target was a 34 ± 9-μg/cm^2 WO_3 deposit at a 45° orientation to the beam. This resulted in a 100-keV (c.m.) energy loss, which is similar to the coherence width.

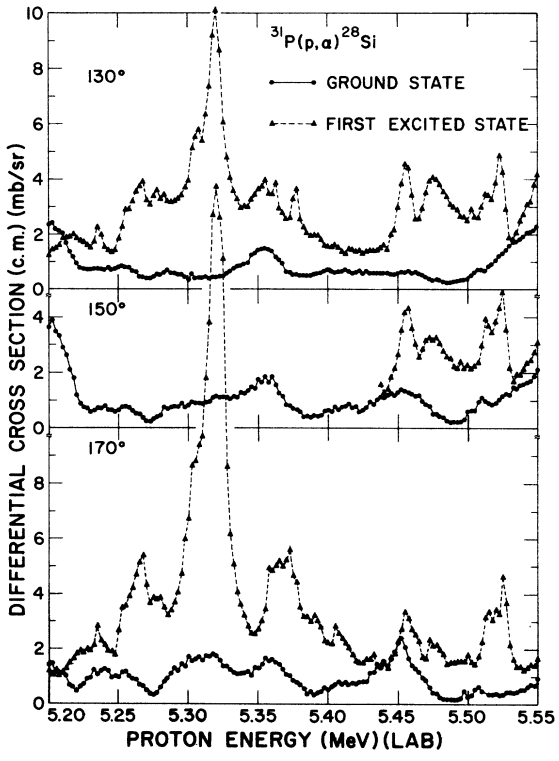

FIG. 1. Excitation functions for the $^{31}P(p,\alpha)^{28}Si$ reactions to the ground state and to the first excited state of ^{28}Si. The limited data for the first excited state at 150° were not analyzed. The proton energy span for the other cases corresponds to compound-nucleus energies from 13.90 to 14.24 MeV.

III. EXPERIMENTAL RESULTS

A. Low-Energy $^{31}P(p, \alpha)^{28}Si$ Cross Sections

The excitation functions obtained for 5.2- to 5.55-MeV proton energy (13.90- to 14.24-MeV compound-nucleus excitation energy) are shown in Fig. 1. The data shown have been corrected for the effect of resolution resulting from target thickness and from beam-energy spread.[21] Evidence for angular cross correlations, particularly for the first excited state, appears in Fig. 1.

Cross correlations between condition 1 and condition 2 are expressed by

$$C_{12}(\epsilon) = \delta[\Delta E(\Delta E - \epsilon)R_1(0)R_2(0)]^{-1/2} \times \sum_{E_i = E_{\min}}^{E_i = E_{\min} + \Delta E - \epsilon} [x_1(E_i) - 1][x_2(E_i + \epsilon) - 1], \quad (3)$$

where δ is the energy increment in the measurements, ϵ is the energy increment in the analysis, and $x(E_i)$ are normalized cross sections $\sigma(E_i)/\langle\sigma(E_i)\rangle$ at energy E_i. The entire energy span is given by ΔE, and $\langle\rangle$ is an average over this span.

The autocorrelations $R(0)$ are similarly

$$R(\epsilon) = \delta[(\Delta E - \epsilon)\Delta E]^{-1/2} \times \sum_{E_i = E_{\min}}^{E_i = E_{\min} + \Delta E - \epsilon} [x(E_i) - 1][x(E_i + \epsilon) - 1] \quad (4)$$

for $\epsilon = 0$. The cross correlations for the data in Fig. 1 are given in Table I. The occurrences of cross correlation approaching unity, particularly for cross correlations between angle for one state, are not surprising. For this reaction even lower orbital angular momenta are involved than in the study of the $^{19}F(\alpha, p)^{22}Ne$ reaction,[22] and for that reaction the angular difference at which the cross correlation decreased to 0.5 is greater than 30°. Since angular cross correlation is expected to be greater[2] for smaller orbital angular momentum, appreciable angular cross correlations are to be expected for the 40° difference between 130 and 170° data. This is evidenced in the excitation function by the persistence of the peak at $E_p = 5.32$ MeV for the first excited state data at both 130 and 170°.

Completely uncorrelated data for particles to different states, but taken over only a finite span of energy, are statistically expected to evidence cross correlations.[21, 22] The data of Fig. 1 represent an undesirably small sample size[25] of $n = 11$ independent energies, and so the cross correlations in Table I between different states are nevertheless consistent with the data being completely uncorrelated between these states. The excitation functions are expected to be uncorrelated since the width-to-spacing ratio Γ/D of compound-nucleus states is greater than unity,[3] which is confirmed by statistical-model calculations discussed in Sec. V. Thus, fluctuation analyses of these data are justified.

B. High-Energy $^{31}P(p, \alpha)^{28}Si$ Cross Sections

The excitation functions obtained for 18.4- to 22.4-MeV protons (26.62- to 30.56-MeV compound-nucleus excitation energy) are shown in Fig. 2. The data shown have been corrected for the effect of resolution resulting from target thickness and from beam-energy spread.[21] The fluctuations in Fig. 2 are obviously superimposed on a moving average. At these energies (considerably above the Coulomb barrier) the repulsive electrostatic effect no longer causes the cross section to increase with energy. Therefore, the cross section is expected to decrease with increasing energy as an increasing number of exit channels are opened.

To analyze these data for fluctuations, the cross section at each energy is normalized to a smooth variation of cross section with energy as in Fig. 2. Curves labeled 0 are $\sigma(E) = B\exp\{-2[a(E_p - 7.6)]^{1/2}\}$ where E_p is the incident proton energy (c.m.). The a value is from Gilbert and Cameron.[19] The B value was determined by a fit to the data. The 7.6-MeV constant gives an approximation to the level density of the final nucleus for low-energy particle emission. To allow for the possibilities of different amounts of direct-reaction cross section σ_{DI} contribution to the observed cross section, curves labeled 3 and 6 are $\sigma(E) = \sigma_{DI} + B\exp\{-2[a(E_p - 7.6)]^{1/2}\}$, with $\sigma_{DI} = 3$ μb/sr and $\sigma_{DI} = 6$ μb/sr, respectively. Again, B was adjusted to fit the data in each case. In these simplifications to provide normalizations, the direct-reaction and compound-nucleus cross sections were taken to be additive.

TABLE I. Cross-correlation values between different conditions in Fig. 1. Cross-correlation values were calculated from (3). Angles are laboratory angles of the data. Reactions to the ground state of ^{28}Si are signified by g.s. and to the first excited state by I.

Condition	Condition 150° g.s.	170° g.s.	130° I	170° I
130° g.s.	0.83	0.04	−0.19	−0.27
150° g.s.		0.39	−0.04	−0.09
170° g.s.				0.43
130° I				0.87

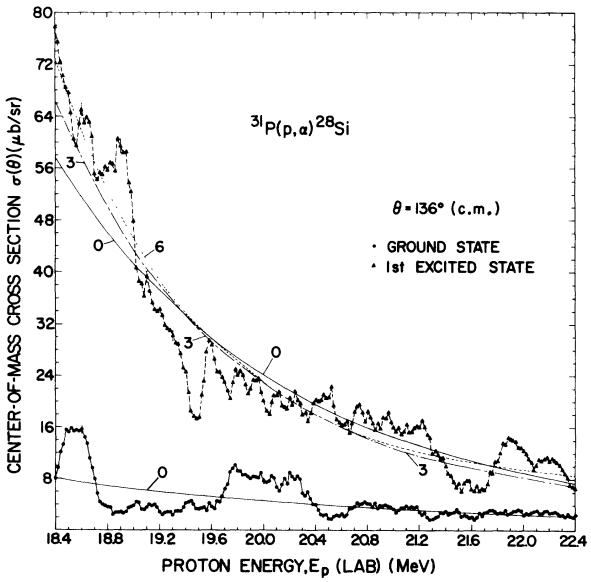

FIG. 2. Excitation functions for the $^{31}P(p,\alpha)^{28}Si$ reactions to the ground state and to the first excited state of ^{28}Si. Curves are normalization curves for the excitation functions. These curves follow $\sigma(E) = \sigma_{DI} + B\exp\{-2 \times [a(E_p - 7.6]^{1/2}\}$ with σ_{DI} equal to 0, 3, and 6 μb/sr for the curves so indicated. See the text in Sec. III B for further details.

Although the width-to-spacing ratio for levels at this compound-nucleus energy is very large, a cross-correlation function was calculated for the ground state and first excited state data. Normalized curves of $\sigma_{DI}=0$ were used for both data. The low $C_{01}(0)=0.07$ for the cross-correlation value confirms that fluctuation analyses are valid.

To test whether the direct-reaction cross section is small compared to compound-nucleus cross sections at the $\theta=136°$ (c.m.) angle of the excitation-function measurements, the angular distributions shown in Fig. 3 were measured. The fact that the cross sections generally do not decrease with increasing angle after $\theta \gtrsim 90°$ indicates that at $\theta=136°$ the cross sections are probably largely compound nucleus.

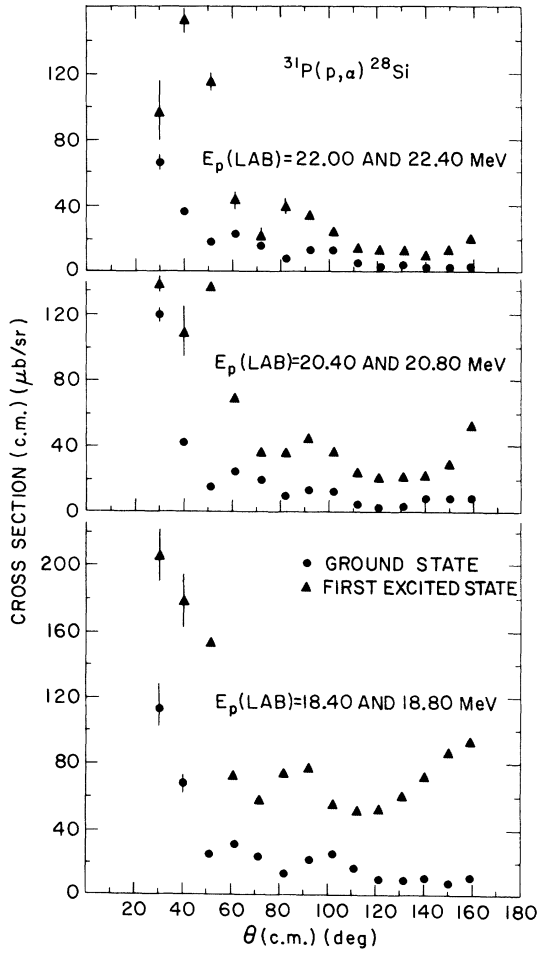

FIG. 3. Angular distributions measured to assure that cross sections for $^{31}P(p,\alpha)^{28}Si$ at backward angles are largely compound-nucleus reactions. This is evidenced by the lack of a general decrease of cross section with increasing angle for $\theta \gtrsim 90°$. The averaging of cross sections for two energies was to decrease any fluctuation effects in the angular distributions. See text in Sec. III B.

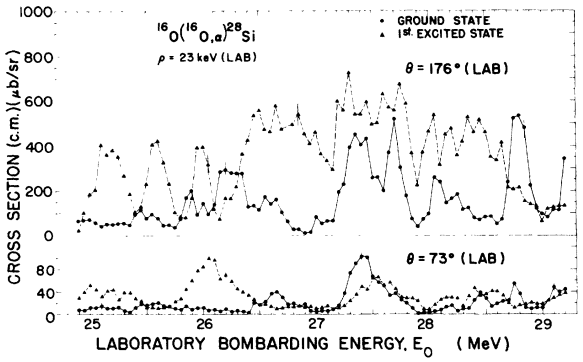

FIG. 4. Excitation functions for the $^{16}O(^{16}O,\alpha)^{28}Si$ reactions to the ground and first excited states of ^{28}Si. The target thickness ρ was thin compared to the coherence width. The data shown have not been corrected for the energy-resolution effects discussed in Sec. III C.

For these angular distributions the target mentioned in Sec. II B was used, and an average of $\sigma(\theta)$ was measured for two energies differing by 400 keV. This difference is ample to assure that energies independent in cross-section fluctuations were involved, thereby reducing the possibility of the angular distribution being a fluctuation rather than an average effect. Actually, the effective number N_{eff} of incoherent amplitudes damping the fluctuations is very close to the limiting value[2] (when half-integer spins are involved) of

$$N=\tfrac{1}{2}(2s+1)(2I+1)(2s'+1)(2I'+1)$$

as a result of the appreciable orbital angular momenta of the high-energy incident protons. Here s is particle spin, I is nuclear spin, unprimed quantities are initial conditions, and primed quan-

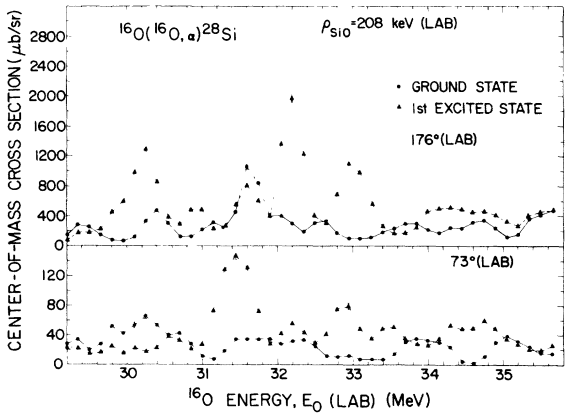

FIG. 5. Excitation functions for the $^{16}O(^{16}O,\alpha)^{28}Si$ reactions to the ground and first excited states of ^{28}Si. The target thickness was approximately the same as the coherence width. The data shown have not been corrected for the energy-resolution effects discussed in Sec. III C.

tities are final conditions. Thus, N_{eff} approaches 2 and 10 for the ground and first excited state reactions, respectively. The use of averaging the cross sections for two energies in Fig. 3 has the effect of increasing these damping numbers to 4 and 20, respectively. This provides considerable damping of fluctuations in these angular distributions.

C. $^{16}O(^{16}O,\alpha)^{28}Si$ Cross Sections

The excitation functions obtained for 24.9- to 29.2-MeV (lab) ^{16}O ions (28.99- to 31.14-MeV compound-nucleus energy) are shown in Fig. 4. For these data, energy loss of the oxygen ions in the target was very small compared to the coherence width, and so these data are used in fluctuation analyses with only small corrections for resolution.

Data were also taken over a wider span of energies with a thicker target. The energy loss of ^{16}O ions in this target was almost the same as the coherence width, and so uncertainties result in determining a coherence width from these data. Although these thick-target data at the lower energies duplicated much of the data in Fig. 4, data for the higher energy span up to 35.75-MeV (lab) ^{16}O energy (34.42-MeV compound-nucleus energy) are shown in Fig. 5. The data in Figs. 4 and 5 are uncorrected for resolution effects, but this correction[21] was made in the fluctuation analyses. For these 31.14- to 34.42- and 29.04- to 34.42-MeV compound-nucleus energy data, it should be emphasized that the resolution correction[21] results in additional uncertainty for these extreme cases where the target thickness is approximately equal to the coherence width.

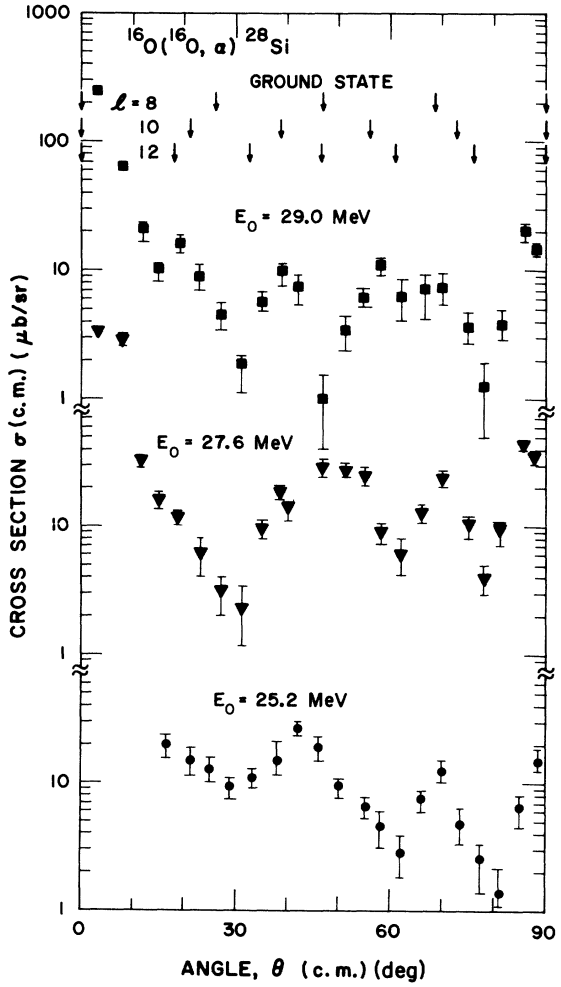

FIG. 6. Measured angular distributions for the ^{16}O-$(^{16}O,\alpha)^{28}Si$ reaction to the ground state. Arrows show the positions of peaks in the $[P_l{}^0(\cos\theta)]^2$ functions.

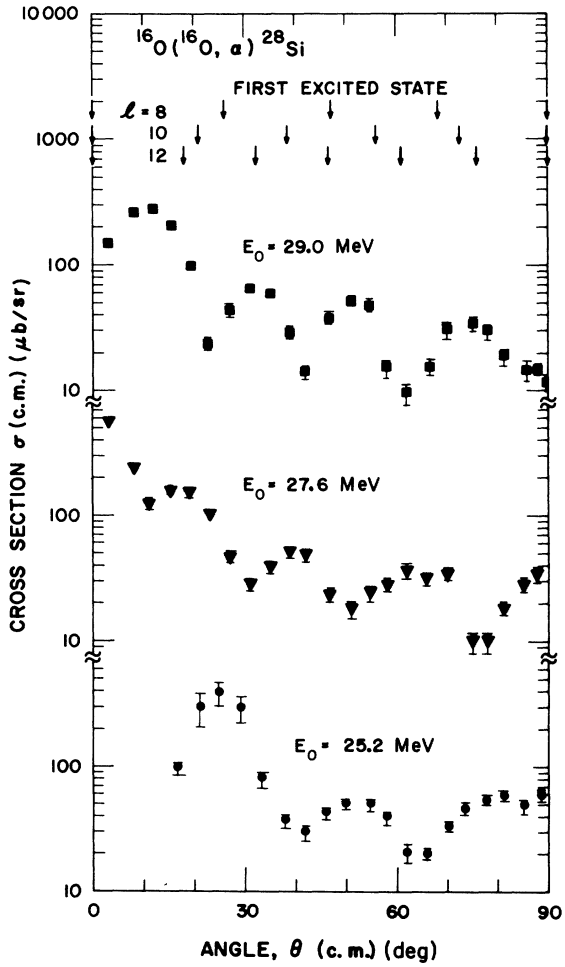

FIG. 7. Measured angular distributions for the ^{16}O-$(^{16}O,\alpha)^{28}Si$ reaction to the first excited state. Arrows show the positions of peaks in the $[P_l{}^0(\cos\theta)]^2$ functions.

Angular distributions of the $^{16}O(^{16}O, \alpha)^{28}Si$ cross section were measured near the upper and lower ends and the midpoint of the 24.9- to 29.2-MeV ^{16}O energy range of Fig. 4. These are shown in Fig. 6 for the ground-state reaction and in Fig. 7 for the first excited state reaction. These data are compared to the angular positions of peaks for the squares of Legendre polynomials $[P_l{}^0(\cos\theta)]^2$, shown as arrows in Figs. 6 and 7. However, the target thickness of about 100 keV (c.m.) is very similar to the coherence width, and so each angular distribution involves only one independent energy. Furthermore, the value of N is low for this reaction, particularly for the $N=1$ case of the ground-state reaction. {For the integer spin case $N=\frac{1}{2}[(2s+1)(2I+1)(2s'+1)(2I'+1)+1].$} Therefore, deviations of measured peaks from the Legendre-polynomial peaks are expected.

IV. FLUCTUATION ANALYSES

A. Coherence Widths

Two methods are used for determining the coherence widths Γ of the compound nucleus.

One method is to analyze the excitation-function data by the autocorrelation functions (4). The coherence width is obtained from

$$R(\epsilon)=\frac{R(0)}{1+\epsilon^2/\Gamma^2}\ , \tag{5}$$

TABLE II. The fractions y of direct reactions and coherence widths measured in the present experiment. The subscripts 0 and 1 on the α in the reactions signify α particles to the ground state and first excited state of ^{28}Si, respectively. The energy span is the ^{32}S compound-nucleus excitation energy covered in the measurements. The sample size n is the number of independent energies covered in the measurements and is found from the average coherence width for both reactions and all angles for each energy span. The coherence width from peak counting is based on two different criteria for a peak: 1σ is for adjacent energy points differing by one standard deviation in the counting statistics, and 2σ is for two standard deviations. Cntg. stat. corr. is the correction of (8) for the counting statistics of the measurement, and samp. size corr. is the correction of (7) for the finite span of energy covered in the measurements.

Reaction	Angle, θ (c.m.) (deg)	Sample size	Fract. of dir. react. y_{min}	y	y_{max}	Coherence width, Γ From peak counting From 1σ (c.m.) (keV)	From 2σ (c.m.) (keV)	From autocorrelation function Corrected Γ (c.m.) (keV)	Cntg. stat. corr. (%)	Samp. size corr. (%)
				$13.90 \le E_{CN} \le 14.24$						
$^{31}P(p, \alpha_0)$	170	11	0.53	0.87	1.00			14.7±2.6	21	10
$^{31}P(p, \alpha_1)$	170	11	0	0	0.12			13.3±2.6	16	10
$^{31}P(p, \alpha_0)$	151	11	0.36	0.67	0.88			8.5±2.6	3	10
$^{31}P(p, \alpha_0)$	131	11	0.32	0.67	0.89			9.3±2.6	2	10
$^{31}P(p, \alpha_1)$	131	11	0	0	0.66			10.6±2.6	1	10
				$26.62 \le E_{CN} \le 30.56$						
$^{31}P(p, \alpha_0)$	136	14				78±8	147±19	95±22	6	5
$^{31}P(p, \alpha_1)$	136	14				98±11	157±20	86±22	9	5
				$28.99 \le E_{CN} \le 31.14$						
$^{16}O(^{16}O, \alpha_0)$	177	11	0	0.55	0.86	90±12	140±24	55±14	9	8
$^{16}O(^{16}O, \alpha_1)$	177	11	0.54	0.85	1.00	71±9	105±17	57±14	11	8
$^{16}O(^{16}O, \alpha_0)$	90	11	0	0	0.57	90±12	158±28	78±14	11	8
$^{16}O(^{16}O, \alpha_1)$	90	11	0	0.21	0.73	97±15	180±34	103±14	28	8
				$31.14 \le E_{CN} \le 34.42$						
$^{16}O(^{16}O, \alpha_0)$	177	12	0.57	0.68	0.77			93±23	0	8
$^{16}O(^{16}O, \alpha_1)$	177	12	0.39	0.59	0.74			97±23	0	8
				$29.04 \le E_{CN} \le 34.42$						
$^{16}O(^{16}O, \alpha_0)$	90	15	0.55	0.70	0.77			109±25	1	6
$^{16}O(^{16}O, \alpha_1)$	90	15	0	0	0.42			136±25	2	6

but two corrections are required for coherence widths obtained by this method. One correction is for the finite sample size[25]

$$n = (\Delta E/\pi\Gamma) + 1 \tag{6}$$

of independent energies in the energy span ΔE measured. For low values of N, a close approximation for this corrected width Γ_{corr} is[21]

$$\Gamma_{\text{corr}} = 2n\Gamma[(n-1)(4n-4+N)]^{-1/2} . \tag{7}$$

As will be shown in Sec. V, variations of coherence width with angle and final state are expected to be small compared to the uncertainties in the width determinations. Therefore, for each energy span, an approximate n is used for all angles and final states. The data in the present work have n values between 11 and 15. For determining coherence widths, these n values result in the moderate sized uncertainties[25] and corrections to the width shown in the summary of results and corrections (Table II).

The coherence width found from (5) is also corrected for the counting statistics of the data. Statistics of a finite number of particles recorded at each energy result in an increase in $R(0)$ of (4), but not in $R(\epsilon)$ for $\epsilon > 0$. With Γ determined from the ϵ for which $R(\epsilon) = R(0)/2$ in (5), the counting-statistics increase in $R(0)$ causes this determination of Γ to be erroneously small. The following method provides an approximate determination of the width corrected for counting statistics. First

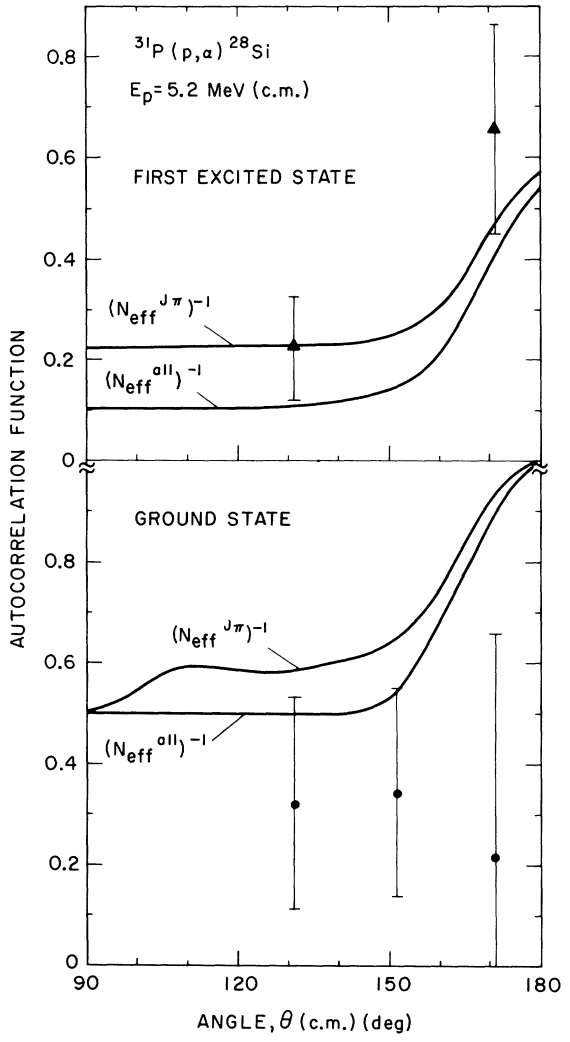

FIG. 8. Autocorrelation functions evaluated at $\epsilon = 0$ compared to calculated numbers of the incoherent amplitudes that damp fluctuations. The autocorrelations $R_0(0)$ shown have been corrected for the finite span of energy measured and for counting statistics. Calculated values of $N_{\text{eff}}{}^{\text{all}}$ are overestimates and of $N_{\text{eff}}{}^{J\pi}$ are underestimates of the true number N_{eff}. See the text of Sec. IV B for details.

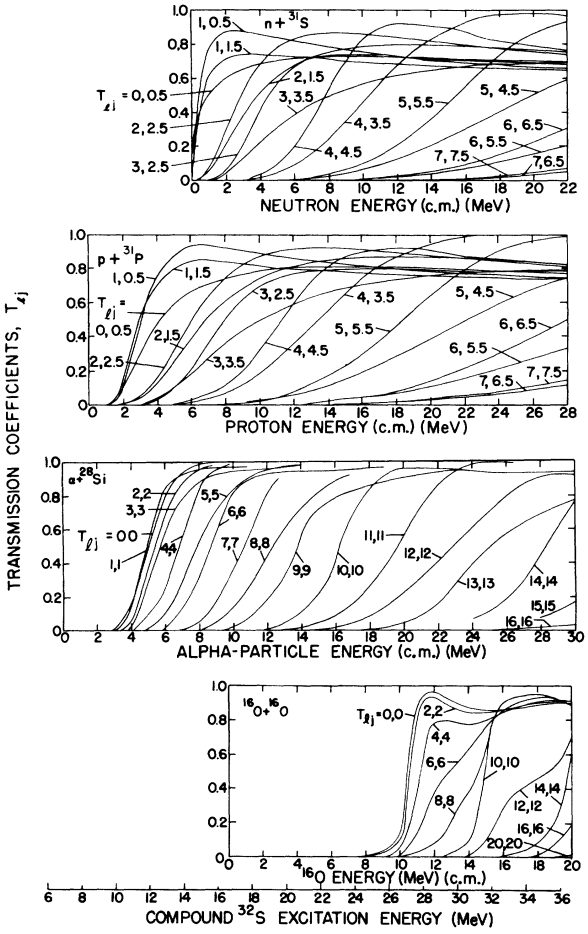

FIG. 9. Transmission coefficients T_{lj} used in calculations made in this paper. These were calculated from the optical model with the parameters of Ref. 30. The channel spin j is given by $\vec{j} = \vec{l} + \vec{s}$. Plots are displaced to a common value of the ^{32}S excitation energy.

the autocorrelation function for $\epsilon = 0$ is corrected for counting statistics. If $\bar{\eta}$ is the average number of particles observed at each energy, then the observed autocorrelation $R(0)$ is related[26] to the autocorrelation $R_0(0)$ for good statistics by $R_0(0) = R(0) - (\bar{\eta})^{-1}$. The coherence width corrected for counting statistics is then approximately

$$\Gamma_0 = \delta \left[\frac{R_0(0)}{R_0(0) - R(\delta)} \right]^{1/2} , \tag{8}$$

where the incremental-energy increase in the measurements, δ, was used, but any small increment ϵ can be used. These corrections are also given in Table II. This correction is large when $R(0)$ is small and when the number of counts is small. As is seen in Table II, this occurs particularly for low-energy ^{31}P(p, α_0)^{28}Si at 170° where $R(0)$ is amolously small and also for the ^{16}O(^{16}O, α)^{28}Si reactions over 28.99- to 31.14-MeV compound-nucleus excitation energy where the number of α particles observed is low.

In Table II, the coherence widths determined from autocorrelation functions for the ^{16}O(^{16}O, α)-^{28}Si reactions are seen to scatter more than the uncertainties, which account only for the uncertainty arising from the finite range of data.[25] Any uncertainties in the appreciable corrections for the counting statistics are not included. Also, no uncertainty is included for the large resolution correction in the oxygen-induced reactions at 31.14- to 34.42- and 29.04- to 34.42-MeV compound-nucleus energy.

Coherence widths for the higher-energy ^{31}P(p, α)-^{28}Si reactions in Table II were determined from data in Fig. 2 after being normalized to the $\sigma_{DI} = 3$ μb/sr line. The width extracted from data with different normalizations increased very slightly with increasing σ_{DI}. These variations were considerably less than the 14-keV uncertainty that results from the sample size n.

Coherence widths were also determined by counting the number K of peaks per unit of energy spanned in the excitation functions. The coherence width is $\Gamma = 0.587/K$, and the uncertainties in Γ were taken from calculations by van der Woude.[27] Two criteria were used to establish a peak in the excitation functions. One was whether a cross section exceeded the average between the cross sections of its neighboring energies by more than the standard deviation of that cross-section measurement. The second criterion was exceeding by twice the standard deviation. As is seen by the results in Table II and as is expected, the 2σ criterion results in considerably larger widths than the 1σ criterion. The latter gives widths similar to those found from autocorrelation analyses. Because of the indefinite nature of establishing the criterion about the definition of peaks, only the widths from autocorrelation functions are used in the following discussions.

B. Fractions of Direct Reactions

Fractions y of direct reactions are determined from autocorrelations, by

$$R_0(0) = (N_{\text{eff}})^{-1}(1 - y^2) , \tag{9}$$

where $y = \sigma_{DI}/(\sigma_{DI} + \sigma_{CN})$ and N_{eff} is the number of incoherent amplitudes effective in damping fluctuations. The autocorrelations $R_0(0)$ corrected for counting statistics were used. These autocorrelation values are shown in Fig. 8 for the low-energy ^{31}P(p, α)^{28}Si reaction. As is seen in the figure, the low number of independent energies, $n = 11$, results in particularly large uncertainties in $R_0(0)$. As noted in Sec. III A, the data at different angles are not independent, and so trends of $R_0(0)$ with angle θ are to be expected. This phenomenon has recently been investigated in depth by Eberhard and Mayer-Böricke.[28]

Also shown in Fig. 8 are calculated values $N_{\text{eff}}^{\text{all}}$ and $N_{\text{eff}}^{J\pi}$ of the number of incoherent amplitudes that damp the fluctuations. As Gibbs has noted,[29] $N_{\text{eff}}^{\text{all}}$ is based on *all* of a very large number of reaction amplitudes contributing to the incoherent amplitudes by

$$N_{\text{eff}}^{\text{all}} = \sum_{\mu} (\bar{\sigma}_{\mu})^2 / (\sum_{\mu} \bar{\sigma}_{\mu})^2 , \tag{10}$$

where $\bar{\sigma}_{\mu}$ are partial cross sections for the μ combination of spin projections in the set $\{s_z, I_z, s_z', I_z'\}$. The $\bar{\sigma}_{\mu}$ values are calculated from the Hauser-Feshbach approximation[17] with the use of the transmission coefficients in Fig. 9. These were calculated by the use of standard parameters[30] with the optical model and by the use of either known levels[31] or a statistical distribution[19] of unknown levels for exit channels.

In the case of ^{31}P(p, α)^{28}Si in Fig. 8, the low particle and nuclear spins result in the calculated $N_{\text{eff}}^{\text{all}}$ being only slightly greater than the true N_{eff}. Another estimate of N_{eff} is provided by the $N_{\text{eff}}^{J\pi}$ calculations, which provide underestimates.[29] For the $N_{\text{eff}}^{J\pi}$ estimate, only the reactions through compound-nucleus states with different $J\pi$ contribute to incoherent amplitudes. As is seen in Fig. 8, the uncertainties in $R_0(0)$ arising from the limited sample size n are very large compared to the uncertainty in the N_{eff} calculations. These $R_0(0)$ values and the calculated $N_{\text{eff}}^{J\pi}$ are used with (9) to calculate the fractions y of direct reactions given in Table II. The values y_{min} and y_{max} result from the statistical uncertainties in $R_0(0)$ determined[25]

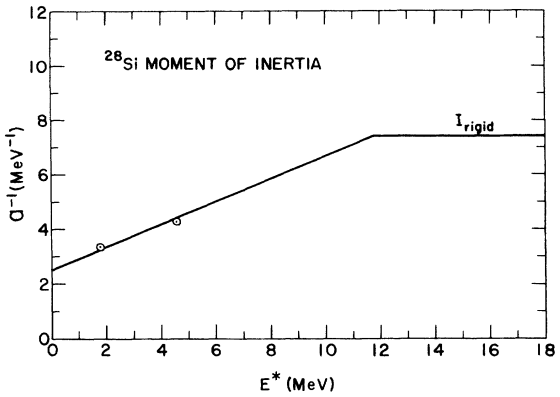

FIG. 10. The inertial parameter of ^{28}Si as used in the width calculations ($a^{-1}=2\vartheta/\hbar^2$). The two circles represent the results of dividing the energies of the first two excited states of ^{28}Si by the appropriate $I(I+1)$ factor.

from the sample size n. (For the oxygen-induced reactions at 31.14- to 34.42- and 29.04- to 34.42-MeV compound-nucleus energy, the large correction for experimental resolution increases the uncertainties in the fraction of direct reactions beyond the values in Table II.) The y results in Table II are inconclusive, but are consistent with a small fraction of direct reactions for these low-energy ^{31}P(p, α)^{28}Si reactions and for the ^{16}O-(^{16}O, α)^{28}Si reactions. One should keep in mind that, as emphasized by Harney and Richter,[32] the use of $N_{\text{eff}}{}^{J\pi}$ results in overestimates of y.

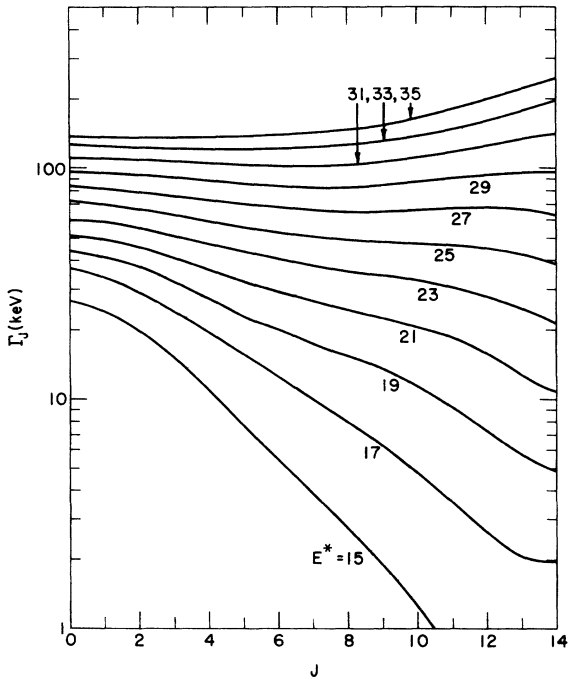

FIG. 11. Calculated values of the coherence width as a function of the compound-nucleus spin J. Calculations were made from (1) with the transmission coefficients of Fig. 9. Statistical model parameters from Ref. 19 were used with the modifications discussed in Sec. V.

V. WIDTH CALCULATIONS

Calculations of nuclear-state widths that correspond to measurements involve calculations of partial widths by (1) and a combination by (2). For these calculations, four quantities require particular attention:

(1) the level densities ρ_r of the residual nuclei;
(2) the level density ρ_{CN} of the compound nucleus;
(3) the transmission coefficients $T_{l,j}$; and
(4) the partial cross sections σ_J.

To minimize the ambiguity in the parametrization of the level density, the expressions and parameters of Gilbert and Cameron[19] were used. These authors used a constant-temperature expression for level densities up to a transition energy and a Fermi-gas expression for higher excitation

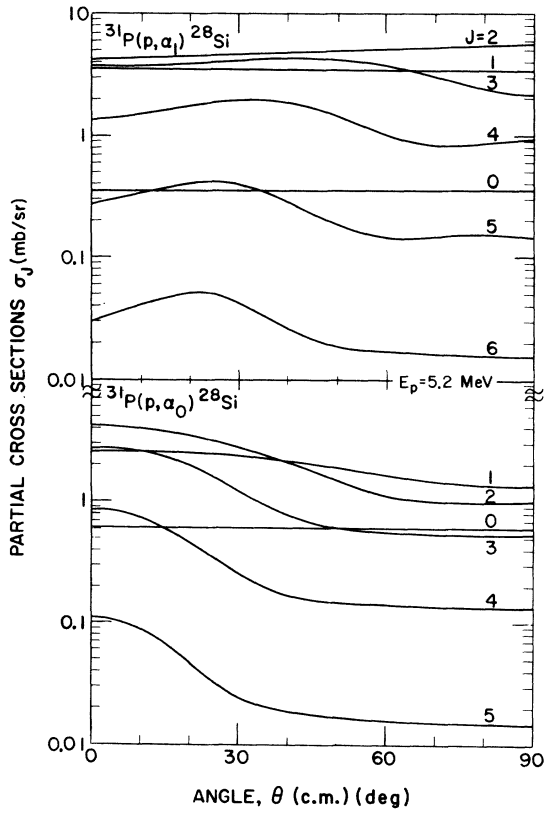

FIG. 12. Partial cross sections σ_J as a function of the angle θ for the reaction ^{31}P(p, α)^{28}Si induced by low-energy protons. These partial cross sections result from Hauser-Feshbach calculations with the transmission coefficients of Fig. 9.

energies. Through their fits to data at low energies, all parameters in the level-density expressions are given. Furthermore, the theoretical variation of level density with nuclear deformation is given.

Some elaboration upon the Gilbert and Cameron level parametrization is desirable for the present case where excitation energies are usually higher than the energies for which the Gilbert and Cameron parameters were determined by fits. One of these elaborations is on the moment-of-inertia parameter, and the other allows different assignments of the nuclear deformation at high excitation energies by means of fits to the width measurements.

The moment-of-inertia parameter enters in the spin-distribution parameter by

$$\rho(I) \propto e^{-(I+\frac{1}{2})^2/2s^2}, \tag{11}$$

where the spin-distribution parameter S is related to the moment of inertia $\mathcal{I}$ by $S^2 = \mathcal{I}t/h$. Here, t is the nuclear temperature. The Gilbert and Cameron values of S were derived from simple considerations of the shell model. However, results of other fluctuation analyses indicate that reduced moments of inertia are needed,[4,7] particularly for the residual nuclei in lower-energy cases.[6]

This increase of moment of inertia with increasing excitation energy is known in greater detail from other studies. At zero excitation energy the moment of inertia is known[33] to be one third of rigid, $\mathcal{I}_{\text{rigid}}/3$. The square of the spin-distribution parameter, S^2, is expected to increase linearly with excitation energy up to a transition energy.[34] We take this transition energy to be the Gilbert and Cameron transition energy between constant temperature and Fermi-gas-level distributions. Above this transition energy the moment of inertia is considered to be rigid, $\mathcal{I} = \mathcal{I}_{\text{rigid}}$. This is illustrated in Fig. 10 for ^{28}Si, where this plot of the inverse parameter $\mathfrak{A}^{-1}$ (where $\mathfrak{A}^{-1} = 2\mathcal{I}/\hbar^2$) agrees

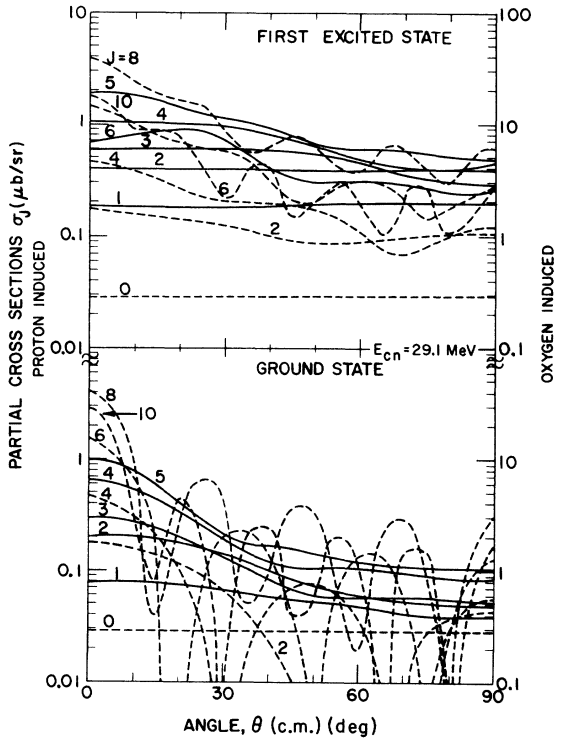

FIG. 13. Comparison of the partial cross sections for ^{31}P(p,α)^{28}Si (solid curves) and ^{16}O(^{16}O,α)^{28}Si (dashed curves) for the same 29.1-MeV compound-nucleus energy. See the text in Sec. V and the caption to Fig. 12 for further details.

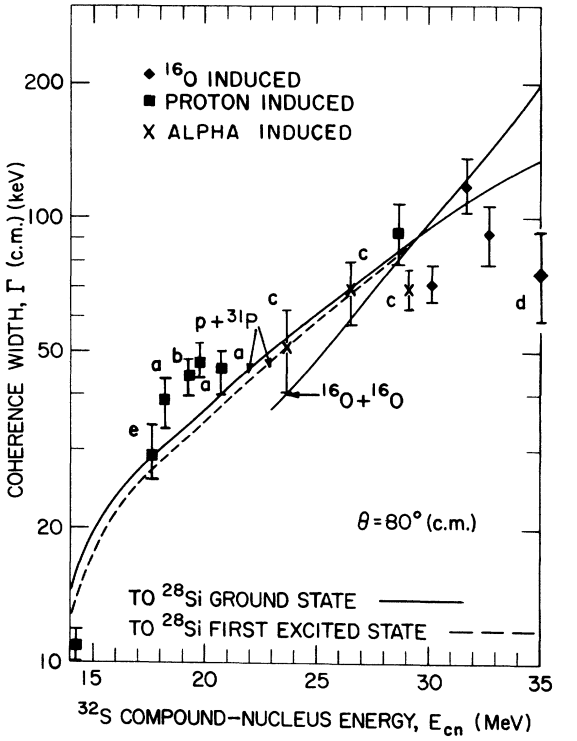

FIG. 14. Variation of ^{32}S coherence width with compound-nucleus excitation energy. The curves are our calculations for ^{31}P(p,α)^{28}Si and ^{16}O(^{16}O,α)^{28}Si at 80° (c.m.). Results at other angles are essentially the same. The data are averaged over final-state reactions and over angles for each energy span. ^{16}O-induced results are shown as diamonds, proton-induced results as squares, and α-induced results as crosses. For all data except point e, which is the result of ^{31}P(p,p_0)^{31}P by Hellström and Dallimore (Ref. 8), the detected outgoing channel was $\alpha + ^{28}$Si. Points a are from Vonach, Katsanos, and Huizenga (Ref. 4), point b is from Dallimore and Allardyce (Ref. 5), points c are from Roeders (Ref. 7), and point d is from Shaw *et al.* (Ref. 6). See Sec. V of text for further details.

well with the inverse inertial parameter derived from dividing the energies of the first two excited states by $I(I+1)$. This comparison is significant since the partial cross sections σ_J to ^{28}Si are particularly important and involve decay to lower excitation energies.

The transmission coefficients T_{lj} were determined by optical-model calculations[30] and are shown in Fig. 9. [A different evaluation of width than given by (1) is obtained by substituting[35]

$$-\ln(1-T) \tag{12}$$

for the transmission coefficient T in (1). However, this correction due to Moldauer[35] gives results very similar to the use of T for our calculations. The smallness of this correction is no doubt due to the fact that, because of the rapid increase of the level-density function, most of the contribution to the width comes from the escaping particles with low energy and hence small transmission coefficients. For the same reason, i.e., most of the decay leads to highly excited states of the final nucleus, no correction was made for the possible effects of direct-reaction contributions.]

The widths Γ_J calculated from (1) with a substitution of (12) are shown in Fig. 11 for the dominant exit channels to ^{28}Si and to ^{31}P. (Widths from ^{16}O and neutron exit channels are lower by at least an order of magnitude.) Comparison of the Γ_J results of Fig. 11 with other published calculations is interesting, even though direct comparisons cannot readily be made as is emphasized in the Introduction. At about 21-MeV excitation energy, Γ_J decreases with increasing J as is found in Fig. 7 of Vonach, Katsanos, and Huizenga,[4] but their rate of decrease is almost twice as much. Similarly, the calculation of Marcazzan and Colli[36] at 19.9 MeV excitation decreases twice as rapidly as ours does. At about 35-MeV excitation energy, Γ_J in Fig. 11 is nearly constant with J for low J, but increases with J in the region of interest. However, Fig. 9 of Shaw *et al.*[6] shows that they calculate a considerable decrease of Γ with J for less than rigid final nuclei. Our results of Fig. 11 will lead to a greater increase of width with increasing energy for high-spin reactions than for low-spin reactions. This is contrary to the results calculated by Eberhard and Richter[14] and by Roeders,[7] both with rigid moments of inertia. Some of these differences are certainly due to our using the variable moment of inertia of Fig. 10.

The widths Γ_J are combined with partial cross sections σ_J by (2). These partial widths were calculated by the Hauser-Feshbach approximation, and the results are shown in Figs. 12 and 13. In these calculations the total number of exit channels was limited to 40. For lower compound-nucleus energies, all known[31] levels of final nuclei could be used. For higher compound-nucleus energies, level densities given by the statistical model[19] were used to extend beyond known levels; level densities were divided by appropriate numbers to reduce the total number of exit channels to the limit of 40.

The calculated variation of the width Γ is shown in Fig. 14 along with widths measured by us and others. [We made no calculations for ^{28}Si(α, α) and ^{31}P(p, p) with which to compare the data points c[7] and e[8] of Fig. 14. However, the angular momenta involved are not too different from those for ^{31}P(p, α), so the $p+^{31}$P calculation provides a good comparison.] This agreement of calculated widths with measured widths is achieved by assuming the level density for the highly excited ^{32}S nucleus corresponds to the Gilbert and Cameron expression for a spherical nucleus. (For the residual nuclei, where the excitation regions of interest are not so high, the Gilbert and Cameron expression for deformed nuclei was used.) The distortion of highly excited nuclei is not well known, but the level density can be expected on the basis of single-particle model calculations to change with distortion.[37] Therefore, the present result of an undeformed nucleus for the highly excited compound nucleus could possibly be real, rather than a compensation for inadequacies in the parameters and computation in the calculated widths. The total uncertainty of the calculated widths arising from sources not associated directly with the level-density expression is estimated to be $\lesssim 10\%$.

VI. CONCLUSION

It has been found that, for the reactions studied, the magnitude, variation with energy, and variation with angular momentum of the total width can be understood in terms of simple statistical models assuming the nuclei concerned are spherical at high excitation, and provided the moment of inertia of the nucleus is assumed to have a certain behavior. While the determination of this behavior is by no means unique it seems very reasonable. We may note that in Fig. 14 the heavy-ion curve intersects with the light-particle curve. The variation of the nuclear parameters ($\mathfrak{a}$, a, etc.) would cause this intersection to be displaced in energy. Thus one might believe that a change in the behavior of the nuclear parameters in one or more of the nuclei involved in the decay of ^{32}S would explain the unexpected results observed. This approach has some validity but it seems that another difficulty looms immediately. The heavy-ion

curve has a strong energy dependence (stronger than the light-particle curve), but the observed widths in ^{32}S from heavy-ion bombardment are almost independent of energy. This casts some doubt on the Γ_J dependencies of Fig. 11. However, a severe change in these dependencies to yield agreement between heavy-ion data and calculations would alter the excellent agreement of the light-particle data with calculations shown in Fig. 14. In addition, such a procedure requires abandoning the good fits to low-energy level-density data which the Gilbert and Cameron level-density expressions provide. It is interesting that Refs. 6, 13, and 14, where a variety of prescriptions for the moment of inertia (all different from ours) are used, show calculated widths for heavy-ion reactions nearly constant with energy at high excitation.

It seems that the understanding of the ^{32}S dilemma is still somewhat distant. However, the understanding of the dependence of width on angular momentum in general has been increased.

ACKNOWLEDGMENTS

The authors appreciate assistance from J. Gursky and L. Allen in source preparations, from M. Peacock and C. Flock in data analysis, and from the operators of the Van de Graaff facility.

---

*Work performed under the auspices of the U.S. Atomic Energy Commission.

†Present address: Defense Nuclear Agency, Washington, D. C. 20305.

‡Present address: Physics Department, Oregon State University, Corvallis, Oregon.

[1]E. Gadioli and L. Zetta, Phys. Rev. 167, 1016 (1968).

[2]T. Ericson, Phys. Letters 4, 258 (1963); D. M. Brink and R. O. Stephen, *ibid.* 5, 77 (1963).

[3]P. J. Riley, G. A. Lock, J. A. Rawlins, and Y. M. Shin, Nucl. Phys. A96, 641 (1967).

[4]H. K. Vonach, A. A. Katsanos, and J. R. Huizenga, Nucl. Phys. A122, 465 (1968).

[5]P. J. Dallimore and B. W. Allardyce, Nucl. Phys. A108, 150 (1968).

[6]R. W. Shaw, Jr., J. C. Norman, R. Vandenbosch, and C. J. Bishop, Phys. Rev. 184, 1040 (1969).

[7]J. D. A. Roeders, Ph.D. thesis, University of Groningen, 1971 (unpublished).

[8]J. Hellström and P. J. Dallimore, Nucl. Phys. A125, 684 (1969).

[9]J. Borggreen, B. Elbeck, and R. B. Leachman, Kgl. Danske Videnskab. Selskab, Mat.-Fys. Medd. 34, No. 9 (1964).

[10]E. Almquist, J. A. Kuehner, D. McPherson, and E. W. Vogt, Phys. Rev. 136, B84 (1964).

[11]G. M. Temmer, Phys. Rev. Letters 12, 330 (1964).

[12]See R. V. Elliott and R. H. Spear, Nucl. Phys. 84, 209 (1966) for a summary of ^{27}Al$(p,\alpha)^{24}$Mg, ^{27}Al(p,n')-^{27}Al*, and ^{27}Al$(p,n)^{27}$Si fluctuation measurements.

[13]See J. D. A. Roeders, L. W. Put, A. G. Drentje, and A. van der Woude, Lettere Nuovo Cimento 2, 209 (1969) for a summary of ^{27}Al$(p,\alpha)^{24}$Mg, ^{12}C$(^{16}$O$,\alpha)^{24}$Mg, and ^{24}Mg$(\alpha,\alpha')^{24}$Mg* fluctuation measurements.

[14]K. A. Eberhard and A. Richter, Bull. Am. Phys. Soc. 15, 570 (1970).

[15]P. Fessenden, W. R. Gibbs, and R. B. Leachman, Phys. Rev. C 3, 807 (1971).

[16]P. Fessenden, W. R. Gibbs, and R. B. Leachman, Phys. Rev. Letters 15, 796 (1965). This equation may be derived by an approximation to the usual method of obtaining the autocorrelation function but not in any entirely satisfactory manner. The simplest derivation is a classical one. The average lifetime of a process going by several independent paths (each with an associated lifetime) is the sum of the separate lifetimes weighted with the probability of the appropriate path. Writing this expression in terms of decay rates, we obtain Eq. (2).

[17]W. Hauser and H. Feshbach, Phys. Rev. 87, 366 (1952).

[18]For example, see D. W. Lang and K. J. Le Couteur, Nucl. Phys. 13, 32 (1959) for a discussion of level densities.

[19]A. Gilbert and A. G. W. Cameron, Can. J. Phys. 43, 1446 (1965).

[20]K. A. Eberhard, P. von Brentano, M. Böhning, and R. O. Stephen, Nucl. Phys. A125, 673 (1969).

[21]G. Dearnaley, W. R. Gibbs, and R. B. Leachman, and P. C. Rogers, Phys. Rev. 139, B1170 (1965).

[22]G. G. Seaman, R. B. Leachman, and G. Dearnaley, Phys. Rev. 153, 1194 (1967).

[23]We thank A. A. Katsanos, J. K. Vonach, and J. R. Huizenga, for providing this ^{31}P target from Argonne National Laboratory. This same target was used for the work of Ref. 22 for ^{31}P$(\alpha,p)^{34}$Cl cross-section measurements. The ^{31}P thickness has now been determined by cross calibration with the ^{31}P target used at high energy. The phosphorus content of the latter target was measured by C. M. Fowler by chemical separation and weighing after completion of the experiment. The fact that the ^{31}P thickness in the former target is less than the 20 μg/cm^2 cited in Ref. 22 means that cross sections reported there should be increased by 45%.

[24]M. L. Halbert, F. E. Durham, C. D. Moak, and A. Zucker, Nucl. Phys. 47, 353 (1963); M. L. Halbert, F. E. Durham, C. D. Moak, and A. Zucker, Phys. Rev. 162, 919 (1967).

[25]W. R. Gibbs, Phys. Rev. 139, B1185 (1965).

[26]W. R. Gibbs, Los Alamos Scientific Laboratory Report No. LA 3266, 1965 (unpublished).

[27]A. van der Woude, Nucl. Phys. 80, 14 (1966).

[28]K. A. Eberhard and C. Mayer-Böricke, Nucl. Phys. A142, 113 (1970).

[29]W. R. Gibbs, Phys. Rev. 153, 1206 (1967).

[30]Parameters for protons and neutrons were from L. Rosen, J. G. Beery, A. S. Goldhaber, and E. H. Auerbach, Ann. Phys. (N.Y.) 34, 96 (1965); parameters for α particles were from R. H. Bassel, G. R. Satchler, R. M. Drisco, and E. Rost, Phys. Rev. 128, 2693 (1962); and parameters for ^{16}O were from J. A. Kuchner and

E. Almquist, in *Proceedings of the Third Conference on Reactions between Complex Nuclei,* edited by A. Ghiorso, R. M. Diamond, and H. E. Conzett (Univ. of California Press, Berkeley, 1963), p. 11.
[31]P. M. Endt and C. Van der Leun, Nucl. Phys. 34, 1 (1962).
[32]H. L. Harney and A. Richter, Phys. Rev. C 2, 421 (1970).
[33]S. G. Nilsson and O. Prior, Kgl. Danske Videnskab. Selskab, Mat. – Fys. Medd. 32, No. 16 (1960).
[34]J. J. Griffin, in *Proceedings of the International Conference on Nuclear Structure, Kingston, 1960,* edited by D. A. Bromley and E. W. Vogt (Univ. of Toronto Press, Toronto, 1960); Phys. Rev. 132, 2204 (1963).
[35]P. A. Moldauer, Phys. Rev. 157, 907 (1967).
[36]M. G. B. Marcazzan and L. M. Colli, Progr. Nucl. Phys. 11, 145 (1969).
[37]L. G. Moretto, Phys. Letters 34B, 191 (1971); L. G. Moretto and R. Stella, *ibid.* 32B, 558 (1970).

PHYSICAL REVIEW C VOLUME 6, NUMBER 4 OCTOBER 1972

Energy Dependence of Elastic α-Particle Scattering: Microscopic Model

G. M. Lerner, J. C. Hiebert, and L. L. Rutledge, Jr.
Cyclotron Institute, Texas A&M University, College Station, Texas 77843*

and

A. M. Bernstein†
Physics Department and Laboratory for Nuclear Science, Massachusetts Institute of Technology, Cambridge, Massachusetts 02139

(Received 8 June 1972)

The energy dependence of elastic α scattering from ^{40}Ca between 39.6 and 115.4 MeV is determined using a microscopic optical model. The agreement between theory and experiment improves as the energy increases. We find that both the real and imaginary parts of the optical potential are well described by a strength depending linearly on energy. For the real part the slope is about half the corresponding value for proton scattering; no theoretical estimates of this quantity are presently available.

The α-particle optical potential, $U(r_\alpha)$, has been related to the nucleon density distribution, $\rho(r)$, by the equation[1,2]

$$U(r_\alpha) = \lambda \int \rho(r) V_{\text{eff}}(\vec{r} - \vec{r}_\alpha) d\tau , \quad (1)$$

where

$$\lambda \equiv \lambda_R + i\lambda_I \quad (2)$$

is an empirically determined complex constant. V_{eff} is the effective α-particle–bound-nucleon interaction derived by folding the α-particle form factor with a nucleon-nucleon interaction which fits the low-energy data.[3] It is found to be approximately a Gaussian whose strength is 37 MeV and range is 2.0 fm.[4,5] Because elastic α scattering is sensitive only to the potential over a relatively small region near the diffraction radius, it is possible to absorb the uncertainties in V_{eff} into λ.[5,6]

This model has been applied to the scattering of α particles from 40 to 166 MeV[1,2,5,7-9] and good agreement with experiment has been obtained. Once λV_{eff} has been determined, Eq. (1) can be used to predict the scattering of α particles (in the diffraction region) given a model for $\rho(r)$. Alternatively, the procedure may be inverted to empirically determine $\rho(r)$ in the surface region.[2,5,7,8]

The method used to determine λ (at a fixed value of E, the center of mass energy) is from α scattering by ^{40}Ca. This is the heaviest $T = 0$ nucleus, and one can assume $\rho_n \approx \rho_p$ which is obtained from electron scattering. This approximation has been checked using Hartree-Fock densities.[5] It has been assumed that λ is a smooth function of E and independent of A. The latter assumption has been confirmed from $A = 16$ to $A = 40$ by successfully predicting α scattering from several $T = 0$ nuclei at 79 and 104 MeV.[2,7] Although an analysis of existing elastic α-particle-scattering data from ^{40}Ca over the range 31 to 166 MeV[9] confirmed the expected behavior of λ with energy, a gradual decrease of λ_R and increase of λ_I, quantitative information could not be obtained because of systematic differences between data sets obtained in different laboratories.

We have measured elastic α scattering by ^{40}Ca